

Article

Resilience-Oriented Planning of Urban Distribution System Source–Network–Load–Storage in the Context of High-Penetrated Building-Integrated Resources

Sheng Zhu ¹, Ping Wang ¹, Wei Lou ^{2,*}, Shilin Shen ¹, Tongtong Liu ¹, Shu Yang ¹, Shizhe Xiang ³ and Xiaodong Yang ^{3,*}

¹ Bengbu Power Supply Company of State Grid Anhui Electric Power Co., Ltd., Bengbu 233000, China

² Electric Power Research Institute of State Grid Anhui Electric Power Co., Ltd., Hefei 230601, China

³ Anhui Province Key Laboratory of Renewable Energy Utilization and Energy Saving, Hefei University of Technology, Hefei 230009, China

* Correspondence: louw0411@ah.sgcc.com.cn (W.L.); yang_xd90@163.com (X.Y.)

Abstract: Building-integrated flexible resources can offer economical availability to accommodate high-penetrated renewable energy sources (RESs), which can be potentially coordinated to achieve cost-effective supply. This paper proposes a resilience-oriented planning model of urban distribution system source–network–load–storage in the context of high-penetrated building-integrated resources. In this model, source–network–load–storage resources are cost-optimally planned, including the lines, soft open point (SOP), building-integrated photovoltaics (BIPVs), building-integrated wind turbine (BIWT), building-integrated energy storage system (ESS), etc. To enhance fault recovery capability during extreme faults, fault scenarios are incorporated into the distribution system operation via coupled multiple recovery stages. The resilience-oriented planning is a thorny problem due to its source–network–load–storage couplings, normal-fault couplings, etc. The original resilience-oriented planning is reformulated as a mixed-integer linear programming (MILP) problem, which can then be solved with a two-stage method and evaluated via a multi-dimensional evaluation metrics. The proposed planning methodology is benchmarked over a Portugal 54-node urban distribution system to verify the superiority and effectiveness on the system economy and resilience levels. Case studies show that the proposed methodology can exploit the optimal synergies of different source–network–load–storage components and enhance system dispatchability.

Keywords: building-integrated resources; urban distribution system; economic optimization; renewable energy



Citation: Zhu, S.; Wang, P.; Lou, W.; Shen, S.; Liu, T.; Yang, S.; Xiang, S.; Yang, X. Resilience-Oriented Planning of Urban Distribution System Source–Network–Load–Storage in the Context of High-Penetrated Building-Integrated Resources. *Buildings* **2024**, *14*, 1197. <https://doi.org/10.3390/buildings14051197>

Academic Editor: Antonio Caggiano

Received: 10 October 2023

Revised: 13 November 2023

Accepted: 22 November 2023

Published: 23 April 2024



Copyright: © 2024 by the authors. Licensee MDPI, Basel, Switzerland. This article is an open access article distributed under the terms and conditions of the Creative Commons Attribution (CC BY) license (<https://creativecommons.org/licenses/by/4.0/>).

1. Introduction

1.1. Background and Motivation

The worldwide low-carbon and zero-carbon policies have powerfully pushed the formulation of smart cities and smart buildings, along with the rapid development of big data and artificial intelligence technologies [1]. Building-integrated resources are energy products or systems which are directly or indirectly integrated with the building or building components, such as façades, roofs, or windows. These energy products or systems are generations and energy storage, such as photovoltaics (PVs), wind turbines (WTs), energy storage systems (ESSs), etc. It is obvious that building-integrated resources can offer economical flexibility to accommodate high-penetrated renewable energy sources (RESs).

In the process of urbanization and building upgrade, a reliable energy supply scale is an important evaluation indicator which has a direct impact on urban socio-economic development [2,3]. How to improve the reliable energy supply scale of urban distribution systems and to decarbonate the whole energy processes have become hot-button issues.

Therefore, it is necessary to scientifically and reasonably plan the urban distribution system source–network–load–storage in the context of high-penetrated building-integrated resources so as to meet urban socio-economic developments.

1.2. Literature Review

Urban distribution system planning in the context of high-penetrated building-integrated resources includes building-integrated photovoltaics (BIPVs), building-integrated wind turbines (BIWTs), building-integrated ESSs, distribution networks, etc. So far, extensive research has investigated coordinated urban distribution system planning, including building physics, the source–network, network–storage, etc.

In the aspect of building physics, the building energy models can be mainly divided into data-driven, high-fidelity physical, and R-C models. Data driven models are obtained based historical data fitting, which cannot ensure prediction accuracy [4]. Various machine learning methods have recently been introduced, though they require large amounts of training data with varying conditions. High-fidelity physical models are based on TRNSYS, DOE-2, EnergyPlus, etc., and originate from the 1980s and also require historical data. These models are often too large and complex and can only be used offline due to their being computationally intractable. Based on the lumped parameter method, R-C models can overcome the above shortages so that analytical optimization can be applied [5]. Based on the R-C thermodynamic model, a robust model predictive control is proposed in [6] to participate in the ancillary market. In [7], heterogeneous buildings are aggregated as microgrids to participate in local energy markets.

In the source–storage aspect, the complementarities of PVs and WTs are exploited via various storage devices (i.e., pumped storage [8], ESSs [9,10]) for zero-carbon 100% renewable supplies. BIPVs and BIWTs are PV and WT materials that are installed on conventional building materials such as the roof, skylights, or facades [11]. Based on the building energy models, building-integrated microgrids can be formulated with BIPVs and BIWTs to meet the building needs [12], and 100% renewable energy is further conceptualized as an energy hub to exploit their inherent multi-energy flexibility and dispatchability [13]. In [14], the geothermal–solar–wind RESs are formulated as a multi-energy portfolio based on an energy hub, and the Markowitz mean-variance approach is introduced to explicitly estimate the risks related to generation changeability. In the source–load–storage aspect, demand response and load shedding generally are introduced to offer considerable flexibility in supply–demand balance through altering energy usage habits and patterns. In [15], proactive data center demand response is integrated with multi-energy planning to accommodate variable RESs since the batch data can be delayed. Traditional electrical demand-side management has evolved into multi-energy demand-side management [16], which has drawn considerable attention. In [17,18], multi-energy demand response is incorporated into an energy hub, which is further formulated into a multi-objective joint planning and operation model.

In the source–network aspect, location and capacity planning can be generally formulated as a two-stage stochastic mixed-integer nonlinear programming problem by considering the random uncertainties of renewable generation and load demand. In [19], a novel analytical approach is proposed by the efficient performance evaluation of a candidate renewable generation placement decision. Demand response can also be introduced to facilitate the source–network planning. In [20], a bi-level expansion planning model is proposed for distribution networks and renewable energy under a demand-side management framework. In the network–storage aspect, an ESS is adopted for bus voltage regulation and energy cost reduction. In [21], optimal ESS allocations in radial distribution systems are investigated. In [22], water storage capacities and the drainage pumps are exploited to provide spatial–temporal flexibility for distribution systems in rainy climates.

Nowadays, urban distribution systems are experiencing a paradigm shift from passive centralized management to distributed power/electronic management [23]. One of the most popular and effective power/electronic devices is the soft open point (SOP). In

distribution network planning with other building-integrated resources, SOPs are generally placed at normally open points and can offer multiple benefits, including load balancing, voltage support, three-phase balancing, and RES hosting capacity improvement [24]. The optimal siting and sizing of SOPs in distribution systems have drawn huge attention. The effects of SOP location and capacity in distribution systems are investigated in [25]. The joint siting and sizing of SOPs with ESSs and repair crews are studied in [26,27]. In [28], a practical optimal SOP planning method is proposed for the post-fault restoration of a coastal distribution system after a typhoon lands. Until now, urban distribution system planning is mainly limited to parts of source–network–load–storage, including source–storage, source–load–storage, source–network, etc. Also, the research on source–network–load–storage planning in urban distribution systems only focuses on the normal operational scenarios.

Ensuring secure, stable, and reliable operation remains the primary imperative in urban distribution system development. Natural or manmade disasters, especially earthquakes, have destructive effects on distribution systems. It is vital to enhance distribution system resilience for withstanding such disasters. Considering the consequences of severe weather events on distribution networks, a three-stage framework is proposed in [29] for evaluating and improving the resilience of these systems. Instead of simulating fault occurrences, information gap decision theory is introduced in [30] to provide planners with accurate designs and a resilience planning model in the face of natural disasters. Conditional value at risk is introduced in [31] to quantify the risks of system outages and further incorporated into a long-term resilient distribution plan. To make full use of SOPs in resilient distribution systems, a bi-level optimal siting and sizing of SOPs is proposed in [32] and a mechanical mapping model is adopted to evaluate resilience enhancement. In [33], the joint siting and sizing of SOPs with remote-controlled switches (RCSs) is proposed for resilience improvement when encountering faults. In [34], SOPs are adopted as the hardening measure in a defender–attacker–defender tri-level model to improve the system resilience to cyberattacks. However, urban distribution system source–network–load–storage planning to improve system resilience under fault scenarios has never been studied.

1.3. Contribution and Paper Organization

To bridge the gap on resilience planning, this paper proposes a resilience-oriented planning for urban distribution system source–network–load–storage in the context of high-penetrated building-integrated resources. The contributions of this paper are as follows:

(1) While the previous literature is mainly limited to the parts of source–network–load–storage (source–storage [8], source–load–storage [15], source–network [19], etc.), the inherent system availability and dispatchability from other flexible parts cannot be fully exploited. This paper focuses on urban distribution system source–network–load–storage planning. Source–network–load–storage resources, including distribution lines, SOPs, BIPVs, BIWTs, building-integrated ESSs, etc., are optimally and strategically located and configured to achieve cost-effective supply.

(2) Instead of focusing on normal operational scenarios [19] or individual faults [33], this paper involves multiple faults and their effects on urban distribution system planning. This paper innovatively integrates various faults into operational scenarios to reflect the risk cost against extreme weather events. Coupled multiple recovery stages are further designed to accommodate extreme faults and enhance system resilience, resulting in a resilience-oriented plan.

(3) Instead of simply assessing the planning results via economical cost [15], this paper is quantitatively evaluated from multi-dimensional perspectives. Six aspects are developed to obtain the system resilience level, including voltage bias level, fault load loss rate, maximum line load level, average penetration rate, average node fault rate, and maximum load reduction ratio. Based on joint cost-resilience analysis, the superiority and effectiveness of the proposed resilience-oriented plan can further be demonstrated.

(4) Mixed-integer linear programming (MILP) relaxation is adopted to handle the inherent nonconvexities within the source–network–load–storage sources, which ensures convexity-preserving properties and computational performance enhancement.

The rest of this paper is organized as follows: Section 2 presents the source–network–load–storage coordination and recovery stages. Section 3 presents the resilience-oriented planning model and relevant evaluation metrics. Sections 4 and 5 show the case study and conclusions.

2. Problem Formulation

This paper aims to provide guidance for the establishment of a resilient urban distribution system. However, the coordination of source–network–load–storage in the context of high-penetrated building-integrated resources is an exceedingly challenging and intricate problem: (1) on the source side, to realize potential socio-economic benefits, the BIPV and BIWT configuration processes must include resource availability, stakeholders' priorities, careful spatio-temporal uncertainty analysis, project economics, etc.; (2) on the network side, the operational dynamics of SOPs should be appropriately modeled for the better coordination with the network topology and static var generator (SVG); (3) on the load side, developing a rational load shedding strategy for supply–demand balance and network security is also a multifaceted consideration; (4) on the storage side, building-integrated ESSs is limited by high capital cost, community priorities, and permit requirements. Furthermore, the distribution system is highly susceptible to faults, and the fault probabilities of individual lines vary across different scenarios, resulting in the diverse failure combinations. The uncertainties of faulty lines have significantly increased the difficulty of fault localization and restoration in the distribution system. Therefore, urban distribution system source–network–load–storage planning is a complex planning problem characterized by multiple components, the uncertainty of faults, a high degree of flexibility, multiple decision candidates, and comprehensive socio-economic considerations.

To achieve the coordination of urban distribution system source–network–load–storage, this paper aims to (1) formulate a distribution system source–network–load–storage planning model for cost-effective supply and resource allocation; (2) capture the operational scenarios involving multiple faults and develop a comprehensive fault recovery process; (3) provide a tool to help the distribution system operator to analyze the cost-effective resilient solution.

2.1. Source–Network–Load–Storage Coordination in the Context of High-Penetrated Building-Integrated Resources

The coordination of source–network–load–storage in the context of high-penetrated building-integrated resources can fully exploit the inherent flexibility among these components: (1) on the source side, there are inherent complementary characteristics among distributed RESs, such as BIPVs and BIWTs; (2) on the network side, the flexible control features of SOPs significantly enhance the source–load matching capability and the system resilience under unpredictable faults; (3) on the load side, the substantial integration of flexible loads makes the power supply–demand more adaptable, thereby facilitating peak–valley load regulation; (4) on the storage side, building-integrated ESSs enhance the flexibility and controllability of the distribution system, thereby providing energy reserves to withstand unpredictable faults.

Figure 1 illustrates the coordination of source–network–load–storage in the context of high-penetrated building-integrated resources. In the scenarios of normal operation, the load nodes are capable of accessing energy from the building-integrated RESs and the main grid. The integration of SOPs, building-integrated ESSs, and SVGs enhances distribution system flexibility, providing active power transfer and reactive power support capabilities to the surrounding nodes. Such integration would in turn contribute to source–load balance and building/RES integration.

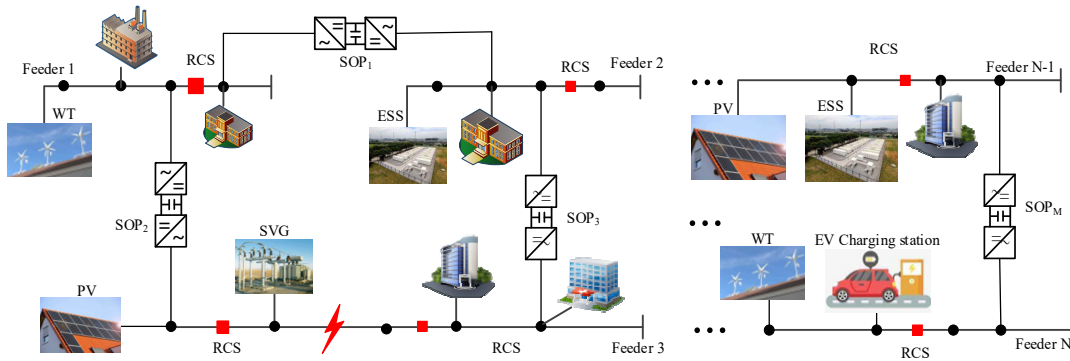


Figure 1. Coordination of source–network–load–storage in the context of high-penetrated building-integrated resources.

Under fault scenarios (assuming a fault occurs on feeder 3), the RCSs located between the faulty line are activated to achieve fault isolation. After the fault has been isolated, the BIPVs located on feeder 3 can be capable of supplying power to the left-side nodes of the fault point, while SOP₂ can be capable of active power transfer to feeder 3. In addition, SOP₂ can offer reactive support to the nearby fault nodes, ensuring voltage support on the fault side and promoting fault restoration. The SOP integration enhances the network interconnection and alters the traditional radial structure, thereby bolstering the resilience and recovery capacity via source–network–load–storage coordination.

2.2. Fault Isolation and Recovery

Figure 2 illustrates the fault propagation and isolation processes. When a fault occurs in one of the lines, the fault will directly propagate to both ends of the line, subsequently impacting the normal operation of the other nodes. Here, the RCSs can promptly detect the fault and be activated to form the minimum outage area after a fault arises, thus minimizing the fault-induced losses. The fault propagation and isolation are represented as (1)–(4), which represent the connection status after the fault and fault state at both ends of the line.

$$(1 - f_{ij,s})(x_{ij} - a_{ij}) \leq x_{ij,T_f,s}^f \leq (1 - f_{ij,s})x_{ij} \quad ij \in \Omega_L \quad s \in \Omega_f \tag{1}$$

$$n_{i/j,T_f,s} \geq f_{ij,s}(1 - a_{ij}) + x_{ij} - 1 \quad ij \in \Omega_L \quad s \in \Omega_f \tag{2}$$

$$n_{i,T_f,s} + x_{ij,T_f,s}^f - 1 \leq n_{j,T_f,s} \quad ij \in \Omega_L \quad s \in \Omega_f \tag{3}$$

$$n_{j,T_f,s} + x_{ij,T_f,s}^f - 1 \leq n_{i,T_f,s} \quad ij \in \Omega_L \quad s \in \Omega_f \tag{4}$$

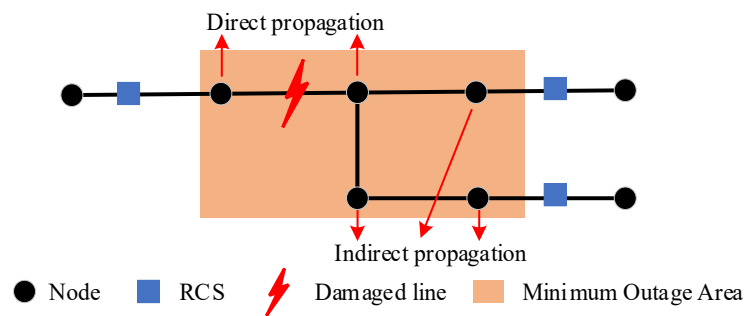


Figure 2. Fault propagation and isolation.

After the fault isolation by the RCSs, it is essential to undertake the fault restoration to recover the power supply of the faulty line. When a node’s fault is caused by a single line failure, the faults can be cleared to restore normal operation once the faulty line is

repaired. When a node's fault is caused by multiple line failures, the fault can only be cleared when all of these lines are repaired. Constrained resource availability, including manpower and equipment, can also limit the restoration pace. Fault restoration complies with constraints (5)–(10). Constraint (5) establishes the maximum count of restored faulty lines. Constraint (6) denotes that the faulty lines will undergo restoration within the stipulated repair duration. Constraints (7)–(10) are imposed on the state of faulty nodes during the repair progress.

$$\sum_{ij} x_{ij,t+1,s}^f - \sum_{ij} x_{ij,t,s}^f \leq R \quad ij \in \Omega_L \quad s \in \Omega_f \quad (5)$$

$$\sum_{t=T_f}^{T_{re}-1} (x_{ij,t+1,s}^f - x_{ij,t,s}^f) = x_{ij} \cdot f_{ij,s} \quad ij \in \Omega_L \quad s \in \Omega_f \quad (6)$$

$$n_{i,t,s} \geq n_{i,t+1,s} \quad i \in \Omega_n \quad s \in \Omega_f \quad (7)$$

$$n_{i/j,t,s} \geq (f_{ij,s} - a_{ij})[(1 - (x_{ij,t,s}^f + x_{ij,t-1,s}^f))] + x_{ij} - 1 \quad ij \in \Omega_L \quad s \in \Omega_f \quad (8)$$

$$n_{i,t,s} + x_{ij,T_f,s}^f - 1 \leq n_{j,t,s} \quad ij \in \Omega_L \quad s \in \Omega_f \quad (9)$$

$$n_{j,t,s} + x_{ij,T_f,s}^f - 1 \leq n_{i,t,s} \quad ij \in \Omega_L \quad s \in \Omega_f \quad (10)$$

3. Resilience-Oriented Planning of Source–Network–Load–Storage

3.1. Resilience-Oriented Planning Objective Function

Resilience-oriented planning can be augmented with a two-stage method and the objective function can be divided into investment/operational costs. The investment costs take one-time capital investments into account:

$$C^{inv} = \sum_{i \in \Omega_{wt}} c_{wt}^{in} WT_i + \sum_{i \in \Omega_{pv}} c_{pv}^{in} PV_i + \sum_{i \in \Omega_{es}} c_{es}^{in} ES_i + \sum_{ij \in \Omega_{sop}} c_{sop}^{in} SOP_{ij} + \sum_{ij \in \Omega_L} c_l^{in} x_{ij} l_{ij} + \sum_{i \in \Omega_{svg}} c_{svg}^{in} SVG_i + \sum_{i \in \Omega_{esub}} c_i^{esub} x_{ei}^{sub} + \sum_{i \in \Omega_{sub}} c_i^{sub} x_i^{sub} + \sum_{ij \in \Omega_{RCS}} x_{ij}^{rcs} c_{rcs}^{in} \quad (11)$$

The annual operational cost comprises two components: maintenance cost and operational cost. The annual maintenance cost is composed of the maintenance expenses related to BIWTs, BIPVs, ESSs, SOPs, SVGs, and lines. Operational cost is constituted by the BIWT and BIPV curtailment cost, ESS degradation cost, electricity purchasing cost, and load shedding.

$$C^{op} = 365 \sum_{t=1}^{24} \sum_{s=1}^S \rho_s \left(\sum_{i \in \Omega_{wt}} f^{wt} P_{i,t,s}^{wtgu} + \sum_{i \in \Omega_{pv}} f^{pv} P_{i,t,s}^{pvgu} + \sum_{i \in \Omega_{es}} f_{es}^{op} (P_{i,t,s}^{ch} + P_{i,t,s}^{dis}) + \sum_{i \in \Omega_{sub} \cup \Omega_{esub}} p_t P_{i,t,s}^{sub} + \sum_{i \in \Omega_n} f_i^n P_{i,t,s}^{cut} \right) + \sum_{i \in \Omega_{wt}} c_{wt}^{op} WT_i + \sum_{i \in \Omega_{pv}} c_{pv}^{op} PV_i + \sum_{ij \in \Omega_{sop}} c_{sop}^{op} SOP_{ij} + \sum_{ij \in \Omega_L} x_{ij} c_l^{op} + \sum_{i \in \Omega_{svg}} c_{svg}^{op} SVG_i \quad (12)$$

In fault scenarios, the fault cost is calculated as the load losses.

$$C^f = \sum_{s=1}^{S_f} \rho_{sf} \left(\sum_{i=1}^n \sum_{t=T_f}^{T_{re}} F_i^{cut} P_{i,t,s}^{Fcut} \right) \quad (13)$$

3.2. Constraints of Source–Network–Load–Storage

(1) Source-side constraints

BIWTs, BIPVs, ESSs, and SVGs need to adhere to the following constraints during their installation and operation:

$$0 \leq WT_i \leq x_i^{WT} WT_i^{\max} \quad i \in \Omega_{wt} \quad (14)$$

$$0 \leq PV_i \leq x_i^{PV} PV_i^{\max} \quad i \in \Omega_{pv} \quad (15)$$

$$0 \leq ES_i \leq x_i^{es} ES_i^{\max} \quad i \in \Omega_{es} \quad (16)$$

$$0 \leq SVG_i \leq x_i^{svg} SVG_i^{\max} \quad i \in \Omega_{svg} \quad (17)$$

$$P_{i,t,s}^{wt,use} + P_{i,t,s}^{wt,gu} = WT_i \cdot P_{i,t,s}^{WT} \quad i \in \Omega_{wt} \quad (18)$$

$$P_{i,t,s}^{pv,use} + P_{i,t,s}^{pv,gu} = PV_i \cdot P_{i,t,s}^{PV} \quad i \in \Omega_{pv} \quad (19)$$

$$0 \leq P_{i,t,s}^{wt,use} \leq (1 - n_{i,t,s}) \cdot WT_i \cdot P_{i,t,s}^{WT} \quad i \in \Omega_{wt} \quad s \in (\Omega_s \cup \Omega_f) \quad (20)$$

$$0 \leq P_{i,t,s}^{pv,use} \leq (1 - n_{i,t,s}) \cdot PV_i \cdot P_{i,t,s}^{PV} \quad i \in \Omega_{pv} \quad s \in (\Omega_s \cup \Omega_f) \quad (21)$$

$$0 \leq \sum_{i=1}^n \sum_{t=1}^T P_{i,t,s}^{wt,gu} \leq \lambda^{WT} \sum_{i=1}^n \sum_{t=1}^T WT_i \cdot P_{i,t,s}^{WT} \quad i \in \Omega_{wt} \quad s \in \Omega_s \quad (22)$$

$$0 \leq \sum_{i=1}^n \sum_{t=1}^T P_{i,t,s}^{pv,gu} \leq \lambda^{PV} \sum_{i=1}^n \sum_{t=1}^T PV_i \cdot P_{i,t,s}^{PV} \quad i \in \Omega_{pv} \quad s \in \Omega_s \quad (23)$$

$$-(1 - n_{i,t,s}) \beta_{\min} SVG_i \leq Q_{i,t,s}^{svg} \leq (1 - n_{i,t,s}) \beta_{\max} SVG_i \quad i \in \Omega_{svg} \quad s \in (\Omega_s \cup \Omega_f) \quad (24)$$

Constraints (14)–(17) represent the maximum installation capacity for BIWTs, BIPVs, and SVGs. Constraints (18)–(21) are the power balance of BIWTs and BIPVs. Constraints (22)–(23) represent the maximum curtailed power for BIWTs and BIPVs. Constraint (24) represents SVG regulation.

In addition to accessing power from RESs, the distribution system operator also draws electricity from the main grid. The expansion planning includes constructing new substations and expanding pre-existing substations. The construction, expansion, and operation constraints of substations are:

$$0 \leq \sqrt{(P_{i,t,s}^{sub})^2 + (Q_{i,t,s}^{sub})^2} \leq (1 - n_{i,t,s}) K^{sub} x_i^{sub} S_i^{sub} \quad i \in \Omega_{sub} \quad s \in (\Omega_s \cup \Omega_f) \quad (25)$$

$$0 \leq \sqrt{(P_{i,t,s}^{sub})^2 + (Q_{i,t,s}^{sub})^2} \leq (1 - n_{i,t,s}) K^{sub} (S_{i0}^{sub} + x_{ei}^{sub} S_{ei}^{sub}) \quad i \in \Omega_{esub} \quad s \in (\Omega_s \cup \Omega_f) \quad (26)$$

Equation (25) represents the operation for constructed substations, while (26) defines the capacity and operation for the pre-existing substation expansion.

(2) Network-side constraints

SOPs with back-to-back converters facilitate the active power exchange between the two terminal feeders and the voltage support. Compared to the conventional radial topology, SOPs enhance distribution system interconnectivity, enabling closed-loop operations. The mathematical constraints for the SOP are presented:

$$0 \leq S_i^{sop} \leq x_{ij}^{sop} S_i^{sop, \max} \quad ij \in \Omega_{sop} \quad (27)$$

$$P_{i,t,s}^{SOP} + P_{j,t,s}^{SOP} + P_{i,t,s}^{SOP,loss} + P_{j,t,s}^{SOP,loss} = 0 \quad (i, j) \in \Omega_{sop} \quad (28)$$

$$P_{i,t,s}^{SOP,loss} = K_i^{SOP} \sqrt{(P_{i,t,s}^{SOP})^2 + (Q_{i,t,s}^{SOP})^2} \quad (i, j) \in \Omega_{sop} \quad (29)$$

$$P_{j,t,s}^{SOP,loss} = K_j^{SOP} \sqrt{(P_{j,t,s}^{SOP})^2 + (Q_{j,t,s}^{SOP})^2} \quad (i, j) \in \Omega_{sop} \quad (30)$$

$$\sqrt{(P_{i,t,s}^{SOP})^2 + (Q_{i,t,s}^{SOP})^2} \leq S_i^{SOP} \quad (i, j) \in \Omega_{sop} \quad (31)$$

$$\sqrt{(P_{j,t,s}^{SOP})^2 + (Q_{j,t,s}^{SOP})^2} \leq S_j^{SOP} \quad (i, j) \in \Omega_{sop} \quad (32)$$

$$-(1 - n_{i,t,s})S_i^{SOP} \leq P_{i,t,s}^{SOP} \leq (1 - n_{i,t,s})S_i^{SOP} \quad i \in (i, j) \in \Omega_{sop} \quad s \in (\Omega_s \cup \Omega_f) \quad (33)$$

$$-(1 - n_{i,t,s})S_i^{SOP} \leq Q_{i,t,s}^{SOP} \leq (1 - n_{i,t,s})S_i^{SOP} \quad i \in (i, j) \in \Omega_{sop} \quad s \in (\Omega_s \cup \Omega_f) \quad (34)$$

Constraints (27) and (28) represent the installation location and active power balance within the SOPs. Constraints (29)–(30) are conversion loss at both ends of the SOPs. Constraints (31)–(32) represent the capacity limitations of the SOPs. (33)–(34) refer to the SOPs' active and reactive power limitations.

Distribution system expansion planning often involves the load nodes and additional lines. The integration of RESs results in the heightened complexity of network planning, possibly leading to the manifestation of looped topologies and isolated nodes. In addition to Constraint (35), additional Constraints (36)–(41) should be introduced to ensure the radial topology.

$$\sum_{ij \in \Omega_L} x_{ij} = N \quad (35)$$

$$0 \leq \sum_{j \in \Omega_n} y_{ij} \leq n - n_{s0}, \quad i \in \Omega_{esub} \quad (36)$$

$$-1 + x_i^{sub} \leq \sum_{j \in \Omega_n} y_{ij} \leq -1 + x_i^{sub}(n - n_{s0}), \quad i = \Omega_{sub} \quad (37)$$

$$\sum_{j \in \Omega_n} y_{ij} = -1, \quad i \in \Omega_n \quad (38)$$

$$|y_{ij}| \leq (n - n_{s0})x_{ij}, \quad (i, j) \in \Omega_L \quad (39)$$

$$0 \leq a_{ij} \leq x_{ij} \quad (i, j) \in \Omega_L \quad (40)$$

$$\sum a_{ij} \leq R_{rcs} \quad (i, j) \in \Omega_L \quad (41)$$

$$0 \leq x_{ij} + x_{ij}^{sop} \leq 1 \quad ij \in \Omega_{sop} \quad (42)$$

Constraint (35) ensures that each newly added node is capable of establishing a new line. Constraint (36) is the maximum virtual power flow that can be dispatched from the existing substation nodes. Constraints (37)–(38) ensure the power flow of the substation node when the node is designated as a newly constructed substation. Constraint (38) denotes that the cumulative virtual flow passing through the node equates to -1 when the node is designated as a load node, signifying the power absorption from the line. Constraint (39) denotes that a line is capable of transmitting virtual flow only when it is constructed. Constraint (40) denotes that RCSs can only be constructed on existing lines. Constraint (41) represents the maximum number for RCS installation. Constraint (42) indicates that SOP installation is prohibited on this line after the construction of line ij .

(3) Load-side constraints

Load shedding strategically reduces or cuts off electricity supply to different consumers or areas in a controlled manner. This process helps balance demand with available

resources. It should be noted that load shedding priority is also considered to simulate the actual scenarios. This equation contains a picture.

$$0 \leq P_{i,t,s}^{cut} \leq \zeta_i P_{i,t,s}^{LOAD} \quad i \in \Omega_n \quad s \in \Omega_s \quad (43)$$

$$0 \leq P_{i,t,s}^{Fcut} \leq P_{i,t,s}^{LOAD} + P_{i,t,s}^{ev} \quad i \in \Omega_n \quad s \in \Omega_f \quad (44)$$

$$0 \leq Q_{i,t,s}^{Fcut} \leq Q_{i,t,s}^{LOAD} \quad i \in \Omega_n \quad s \in \Omega_f \quad (45)$$

Constraint (43) indicates the maximum load shedding during the normal operation. Constraints (44) and (45) represents the active and reactive load shedding during fault scenarios.

Electric vehicle (EV) charging stations are typically found street-side or at retail shopping centers, government facilities, and other parking areas. The EV charging stations can be characterized by (46) and (47).

$$\sum_e x_{e,i}^{ev} = 1 \quad i \in \Omega_{ev} \quad e \in \Omega_{ev,i} \quad (46)$$

$$P_{i,t,s}^{ev} = x_{e,i}^{ev} P_{e,t,s}^{EV} \quad i \in \Omega_{ev} \quad e \in \Omega_{ev,i} \quad (47)$$

Constraint (46) indicates that each charging station can only have one construction node. Constraint (47) represents the power connectivity to node i after the construction of EV charging stations.

(4) Storage-side constraints

ESS is the ability to capture energy at one time for use at a later time. Constraints (48)–(53) represent the operation of ESSs.

$$0 \leq P_{i,t,s}^{dis} \leq (1 - n_{i,t,s}) \cdot \eta_{i,t,s}^{dis} \cdot k_{dis} \cdot ES_i \quad i \in \Omega_{es} \quad s \in (\Omega_s \cup \Omega_f) \quad (48)$$

$$0 \leq P_{i,t,s}^{ch} \leq (1 - n_{i,t,s}) \cdot \eta_{i,t,s}^{ch} \cdot k_{ch} \cdot ES_i \quad i \in \Omega_{es} \quad s \in (\Omega_s \cup \Omega_f) \quad (49)$$

$$\eta_{i,t,s}^{ch} + \eta_{i,t,s}^{dis} = 1 \quad i \in \Omega_{es} \quad (50)$$

$$S_{i,t,s}^{soc} = S_{i,t-1,s}^{soc} + \eta_{ch} P_{i,t,s}^{ch} \Delta t - \frac{P_{i,t,s}^{dis} \Delta t}{\eta_{dis}} \quad i \in \Omega_{es} \quad (51)$$

$$\mu_{min} \cdot ES_i \leq S_{i,t,s}^{soc} \leq \mu_{max} \cdot ES_i \quad i \in \Omega_{es} \quad (52)$$

$$S_{i,1,s}^{soc} = S_{i,24,s}^{soc} \quad i \in \Omega_{es} \quad (53)$$

Constraints (48)–(49) represent the maximum charging and discharging power. Constraint (50) represents the charging and discharging state. Constraints (51)–(53) are the energy capacity limitations.

(5) Power-flow constraints

Distflow [25], which allows us to efficiently compute the active/reactive power flows and voltage drop, is adopted to model the power flow of distribution systems.

$$P_{i,t,s}^{in} + \sum_{ji \in \Omega_L} P_{ji,t,s} - P_{i,t,s}^{LOAD} = \sum_{ij \in \Omega_L} P_{ij,t,s} \quad i \in \Omega_n \quad (54)$$

$$Q_{i,t,s}^{in} + \sum_{ji \in \Omega_L} Q_{ji,t,s} - Q_{i,t,s}^{LOAD} = \sum_{ij \in \Omega_L} Q_{ij,t,s} \quad i \in \Omega_n \quad (55)$$

$$P_{i,t,s}^{in} = P_{i,t,s}^{wt,use} + P_{i,t,s}^{pv,use} + P_{i,t,s}^{sub} + P_{i,t,s}^{SOP} + P_{i,t,s}^{cut} + P_{i,t,s}^{dis} - P_{i,t,s}^{ch} - P_{i,t,s}^{ev} + n_{i,t,s} \cdot P_{i,t,sf}^{Fcut} \quad i \in \Omega_n \quad s \in (\Omega_s \cup \Omega_f) \quad (56)$$

$$Q_{i,t,s}^{in} = Q_{i,t,s}^{svg} + Q_{i,t,s}^{sub} + Q_{i,t,s}^{SOP} + n_{i,t,s} \cdot Q_{i,t,sf}^{Fcut} \quad i \in \Omega_n \quad s \in (\Omega_s \cup \Omega_f) \quad (57)$$

$$U_{i,t,s} - U_{j,t,s} \leq M(1 + f_{ij,s} - x_{ij}) + (r_{ij}P_{ij,t,s} + x_{ij}Q_{ij,t,s})/V_0 \quad ij \in \Omega_L \quad s \in (\Omega_s \cup \Omega_f) \quad (58)$$

$$U_{i,t,s} - U_{j,t,s} \geq M(1 + f_{ij,s} - x_{ij}) + (r_{ij}P_{ij,t,s} + x_{ij}Q_{ij,t,s})/V_0 \quad ij \in \Omega_L \quad s \in (\Omega_s \cup \Omega_f) \quad (59)$$

$$U_{min} \leq U_{i,t,s} \leq U_{max} \quad i \in \Omega_n \quad s \in (\Omega_s \cup \Omega_f) \quad (60)$$

$$0 \leq \sqrt{(P_{ij,t,s})^2 + (Q_{ij,t,s})^2} \leq (x_{ij} - f_{ij,s})S_{ij} \quad ij \in \Omega_L \quad s \in (\Omega_s \cup \Omega_f) \quad (61)$$

Constraints (54)–(55) represent power flow between nodes. Constraints (56)–(57) represent the active and reactive power injections at the nodes. Constraints (58)–(59) indicate the voltage drop between nodes. Constraint (60) corresponds to the voltage range. Constraint (61) represents the line capacity.

3.3. Multi-Dimensional Evaluation

It is a specific, observable, and measurable accomplishment or change that shows the progress made toward achieving a resilience-oriented plan for urban distribution system source–network–load–storage. This paper is quantitatively performed in terms of six aspects to obtain the system resilience level, including voltage bias level, fault load loss rate, maximum line load level, average penetration rate, average node fault rate, and maximum load reduction ratio.

The average voltage deviation reflects the average degree of deviation from its rated value:

$$c_{VEI} = \sum_{s=1}^S \frac{\rho_s}{nT} \sum_{t=1}^T \sum_{i=1}^n \sqrt{(1 - U_{i,t,s}/V_0)^2} \quad (62)$$

The average fault isolation load loss is calculated as the proportion of the load shedding resulting from fault occurrence and fault isolation:

$$c_{FLR} = \sum_{s=1}^{S_f} \rho_{sf} \frac{\sum_{i=1}^n P_{i,Tf,s}^{Fcut}}{\sum_{i=1}^n P_{i,Tf,s}^{LOAD}} \quad (63)$$

The maximum average load rate is defined as the maximum value of the ratio between the line load values and their rated capacities:

$$c_{ALR} = \max\left(\frac{\sum_{ij \in \Omega_L} \sqrt{P_{ij,t,s}^2 + Q_{ij,t,s}^2}}{\sum x_{ij} \cdot S_{ij}}\right) \quad (64)$$

The average penetration rate denotes the proportion of RESs supplied to the load:

$$c_{ARP} = \sum_{s=1}^S \rho_s \frac{\sum_{t=1}^T \sum_{i=1}^n (P_{i,t,s}^{wt,use} + P_{i,t,s}^{pv,use})}{\sum_{t=1}^T \sum_{i=1}^n P_{i,t,s}^{LOAD}} \quad (65)$$

The average fault rate of nodes refers to the proportion of fault nodes to the total number of nodes after fault occurrence:

$$c_{AFR} = \sum_{s=1}^{S_f} \rho_{sf} \frac{\sum_{i=1}^n n_{i,T_f,s}}{n} \quad (66)$$

The maximum load reduction ratio indicates the maximum load reduction during normal scenarios:

$$c_{DRR} = \max\left(\frac{\sum_{i=1}^n P_{i,t,s}^{cut}}{\sum_{i=1}^n P_{i,t,s}^{LOAD}}\right) \quad (67)$$

3.4. MILP Reformulation

The original resilience-oriented planning is hard to solve via available commercial solvers because of its inherent nonconvexities and nonlinearity. Compared to conic and nonlinear programming problems, MILP exhibits a distinct advantage in terms of computational speed. In such cases, the original model is firstly reformulated via the MILP relaxation method for computational simplification.

As for bi-linear terms, McCormick Envelopes [1] provide a straightforward and tight relaxation technique for replacing these terms with a new variable. As an example, the nonlinearity introduced by the bi-linear term $\eta_{i,t,s}^{dis} ES_i$ can be mitigated. The original nonlinear term can be replaced by the variable NES^{dis} and relaxed with the following constraints:

$$0 \leq NES^{dis} \leq \eta_{i,t,s}^{dis} \cdot ES_i^{\max} \quad (68)$$

$$ES_i + \eta_{i,t,s}^{dis} \cdot ES_i^{\max} - ES_i^{\max} \leq NES^{dis} \leq ES_i \quad (69)$$

For second-order cone constraints, a fitted relaxation can be achieved through the polygon's constraints, as shown in Figure 3. Although increasing the edge count enhances computational precision, an overabundance of edges may lead to a substantial increase in computational complexity. When the edge count reaches 16, the relaxation error is approximately 2%, simultaneously ensuring computational accuracy and computational speed.

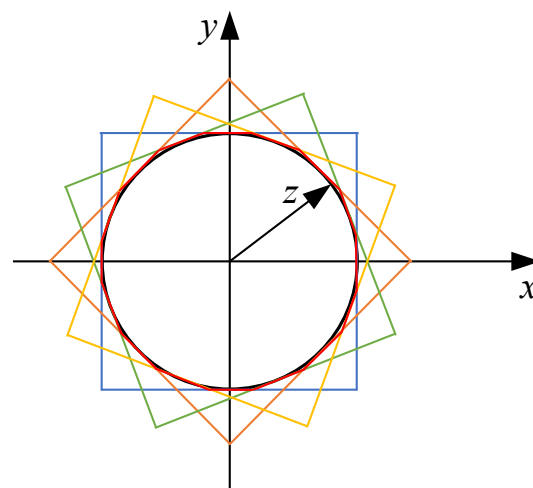


Figure 3. Schematic diagram of second-order cone linearization.

3.5. Two-Stage Planning–Operation Method

By performing the reformulation and linearization in Section 3.4, the original source–network–load–storage planning problem can be transformed into a MILP problem, leading to a notable enhancement in computational efficiency. With the uncertainties of renew-

able generations and faults captured via Monte Carlo simulations, a two-stage stochastic resilience-oriented plan can be developed. In the first stage, the objective is to minimize the total investment. Once the source–network–load–storage capacities and locations are determined, the subsequent stage encompasses the system’s operation cost in the presence of uncertain conditions.

$$\min \left\{ C^{inv} + \frac{(r+1)^x - 1}{r(r+1)^x} (C^{op} + C^f) \right\} \quad (70)$$

All decision-making processes are coded on the YALMIP toolbox [35] of MATLAB 2020B on a workstation with 2.7-GHz AMD Ryzen Threadripper Pro 3995WX CPU and 128GB RAM and solved with the MILP solver CPLEX with its default settings.

4. Case Study

4.1. Base Data

The resilience-oriented plan for the urban distribution system source–network–load–storage in the context of high-penetrated building-integrated resources is tested on a Portugal 54-node system [36]. The standard voltage is 15 kV with a total active power load of 71.6 MW. The system is equipped with a BIWT, BIPVs, ESS, SVG, and SOP, whose baseline installed capacities are set as 1 MW, 1 MW, 0.5 MW, 0.5 MVar, 0.5 MVA, respectively. Suppose lines (4–5, 9–10, 12–13) of the network are originally equipped with RCSs. Candidate nodes for the BIWT, BIPV, SVG, and ESS installation are designated as (13,16,22,24,47), (5,10,30,42,47), (20,32,43,49), and (17,31,35,45). Lines with SOPs are (2–8, 6–28, 10–15, 30–43, 33–39, 46–47, 22–23). Candidate nodes for the EV charging stations are (37,43,45), (9,22,23), (8,33,34), (40,48,50). The purchase costs for substations during peak, normal, and off-peak hours are USD 0.120/KW, USD 0.093/KW, and USD 0.053/KW. The ESS charging/discharging efficiency is 0.9 and the allowable charging/discharging depth in each time slot is 0.2 [16]. The planning period covers 20 years, with a discount rate of 5% for investments. The test case for simulation includes 10 fault scenarios with each scenario consisting of six lines and random faults. Other simulation parameters are all derived from the [15,33,36] and manufacturing suppliers.

In order to validate the performance enhancement, comparative schemes are presented:

- (1) Scheme 1 is the proposed resilience-oriented planning of the urban distribution system source–network–load–storage.
- (2) Scheme 2 is the resilience-oriented planning of the urban distribution system source–network–load–storage without taking SOPs into account.
- (3) Scheme 3 is the resilience-oriented planning of the urban distribution system source–network–load–storage without taking multiple-fault scenarios into account.

4.2. Analysis of Planning Results

Figure 4 and Table 1 depict the planning results of Schemes 1–3. SOPs can perform load transferring and voltage support, enabling prompt fault isolation and service restoration in distribution networks. The contribution of SOP integration to system flexibility, and thus to system dependency on ESSs and SVGs, results in a decrease in installed capacity. Thus, the installed capacities in Scheme 1 for the BIWT, BIPVs, ESS, SVG, and SOP are 41 MW, 64 MW, 20 MW, 2.5 MVar, and 22.5 MVA. These are lower than the corresponding capacities in Scheme 2, which are 45 MW, 68 MW, 25 MW, and 13 Mvar. From the perspective of RCSs, it is observed that RCSs tend to be deployed at both ends of RESs, SOPs, ESSs, and SVGs, as well as upstream of A+ level loads and EV charging stations. It is because RCSs can ensure the operation of RESs, ESSs, and high-level loads in the event of a fault, thereby reducing losses during fault occurrences. From the perspective of EV charging stations, it is observed that EV charging stations tend to be deployed near RESs due to RES accommodation.

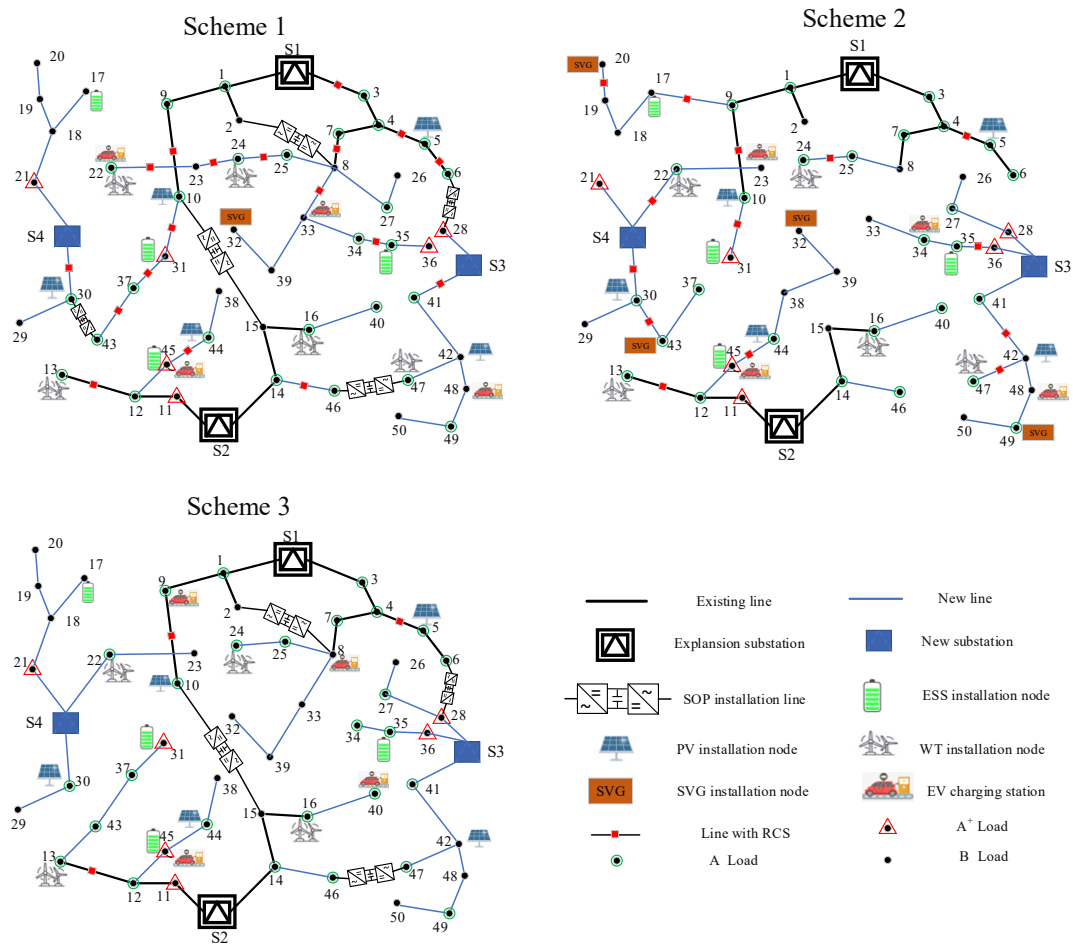


Figure 4. Planning results of Schemes 1–3.

Table 1. Planning results of Schemes 1–3.

Location (Capacity)		Scheme 1					Scheme 2					Scheme 3				
BIPVs (MW)	5	10	30	42	44	5	10	30	42	44	5	10	30	42	44	
	20	15	12	9	11	7	15	13	18	15	14	15	9	13	15	
BIWT (MW)	13	16	22	24	47	13	16	22	24	47	13	16	22	24	47	
	2	9	7	13	10	7	8	6	12	12	15	6	6	15	0	
ESS (MW)	17	31	35	45	17	31	35	45	17	31	35	45	17	31	35	
	4	4	8	4	8	5	8	4	4	4	5	8	5	5		
SVG (MVar)	20	32	43	49	20	32	43	49	20	32	43	49	20	32	43	
	0	0	2.5	0	4	3	3	3	0	0	0	0	0	0	0	
SOP (MVA)	2–8	10–15	30–43	46–47	6–28	/					2–8	10–15	46–47	6–28		
	5	5	3.5	4	5	/					3.5	4.5	2.5	2.5		

In contrast to Scheme 1, the impacts of faults are not considered in Scheme 3, leading to the absence of redundant RCSs. In Scheme 3, the installed capacities for the BIWT, BIPVs, ESS, SVG, and SOP are 42 MW, 66 MW, 22 MW, 0 MVar and 13 MVA. When fault scenarios are not considered, it is evident that the system resilience relies on the SOP, while the SOP is responsible for maintaining the power supply during normal scenarios and voltage support during fault scenarios. In terms of the installed BIWT capacity, there is little difference in the total capacity considering both fault scenarios and normal scenarios. Scheme 1 employs

a more dispersed plan, while Scheme 3 adopts a more centralized plan. This suggests that the RES plan with smaller capacities and dispersed placement is more likely to enhance distribution system resilience.

4.3. Analysis of Operational Results

Table 2 presents the cost comparisons of Schemes 1–3. It can be concluded that Scheme 1 can make full use of the urban distribution system source–network–load–storage coordination in the context of high-penetrated building-integrated resources. From a total cost perspective, Scheme 1 demonstrates a significant cost advantage over Scheme 2, indicating that the SOP can enhance cost-effective operations. Due to the relatively low annual failure probability, the advantage of Scheme 1 over Scheme 3 is not obvious, resulting in a comparatively minor contribution of failure costs to the total cost. Compared with Schemes 1–2, the system costs of the schemes are reduced by 6.7% and 1.0%.

Table 2. Optimized results of Schemes 1–3.

	Scheme 1	Scheme 2	Scheme 3
Obj (10^6 USD)	359.51	385.31	363.25
C^{inv} (10^6 USD)	126.07	133.97	125.10
C^{op} (10^6 USD)	18.37	21.62	18.59
C^f (10^5 USD)	2.21	3.02	5.24
Electricity purchase cost (10^6 USD)/year	15.13	15.52	14.85
Load reduction cost (10^5 USD)/year	3.07	13.86	8.79
BIWT, BIPV curtailing cost (10^5 USD)/year	2.12	3.33	1.66
Battery degradation cost (10^5 USD)/year	3.33	4.79	3.93

For other operational costs, Scheme 1 exhibits superior performance to both Scheme 2 and Scheme 3 in terms of failure loss costs, load reduction costs, and battery degradation costs. This is due to the larger SOP capacity in Scheme 1 improving the interconnectivity and adaptability of the urban distribution system. From the perspective of fault loss costs, Scheme 1 demonstrates a decrease of approximately 26.8% compared to Scheme 2, signifying the ability of SOPs to reduce losses in the event of faults. When considering load shedding costs and battery degradation costs, Scheme 1 significantly outperforms both Scheme 2 and Scheme 3. This is due to its larger SOP planning capacity and enhanced operational flexibility. Furthermore, the source–network–load–storage planning in Scheme 3 is more concerned with normal scenarios, resulting in insufficient system capacity to withstand faults and significant load loss costs. While the planning level of Scheme 3 is required to meet the minimal power supplied criteria, the planning level of Scheme 1 is required to withstand unpredictable faults. Such factors contribute to a few counter-intuitive results, such as electricity procurement costs and the expenses incurred in curtailing BIWTs and BIPVs.

Figure 5 illustrates the SOP power flow of Scheme 1. Due to the low load demands and low output of BIPV generation during hours 0–9, BIWTs are used to meet the load demand with ESSs, resulting in minimal active power transfer through the SOPs. During the high-demand hours 10–22, the SOPs engage in frequent power exchanges to facilitate power coordination between networks and enhance the utilization of RESs. When BIPV generation surpasses BIWT generation during hours 10–16, the SOPs facilitate the absorption and utilization of BIPVs through power interactions. Subsequently, during another high-demand period from hours 17 to 22, substantial electricity procurement is required from the substations as the BIPVs diminish and the BIWT cannot meet the load requirements.

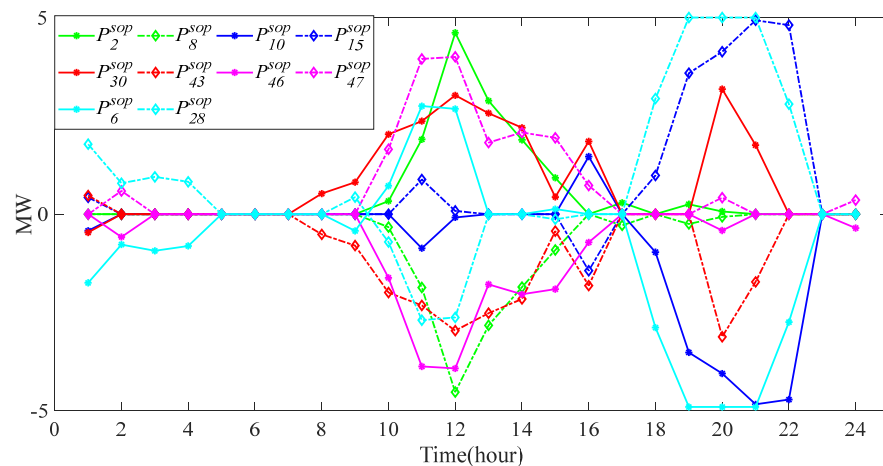


Figure 5. Active power transfer of SOP in Scheme 1.

Figure 6 represents the total electricity procurement. Schemes 1 and 3 exhibit relatively minor disparities and notably outperform Scheme 2 in terms of electricity procurement. This emphasizes the enabling effect of the SOPs in driving and promoting the effective integration of RESs. The integration of the distributed BIWTs, BIPVs, and ESSs has led to a noticeable shift in the supply–demand curve. The initial supply–demand pattern with two peaks and two valleys has transformed into a unimodal pattern with a single peak and a single valley, consequently reducing the peak load demand.

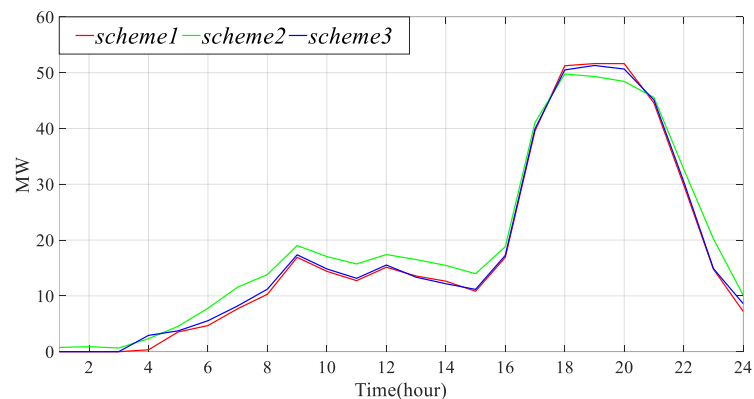


Figure 6. The purchased electricity for Schemes 1–3.

In Table 3, the fault isolation and restoration process for one specific fault scenario is depicted, where faults have occurred in lines 4–5, 12–45, 16–40, 29–30, 33–34, and 41–53. The green-shaded area in the diagram represents operational nodes, while the orange-shaded area denotes the faulty nodes. During the fault isolation phase, Scheme 1 has a smaller fault area compared to Scheme 2, while Scheme 3 has larger fault area due to the absence of redundant RCSs. In the first phase of fault restoration, the repair of faulty lines effectively clears most of the node faults, allowing RESs, ESSs, and SOPs to operate normally. In the second phase of fault restoration, most node faults have been successfully cleared and the load has been almost restored. During the third recovery phase, all faults have been restored, resulting in the system recovery to its normal operational state. From a holistic recovery perspective, Scheme 1 demonstrates a notably lower average node failure rate compared to Scheme 2 and Scheme 3. It should be emphasized that the analysis is limited to a single fault scenario, and this superiority will become even more obvious in the context of multiple scenarios and Scheme 3. Because of the lack of RCS- and SOP-redundant planning, the fault area size is more susceptible to faulty lines.

Table 3. The fault recovery process for Schemes 1–3.

Stage	Scheme 1	Scheme 2	Scheme 3
Isolation stage			
Restoration stage 1			
Restoration stage 2			
Restoration stage 3			

4.4. Multi-Dimensional Comparisons

Based on the multi-dimensional evaluation in (62)–(67) in Section 3.3, Figure 7 presents a radar chart illustrating the multi-dimensional comparisons of Schemes 1–3. It is evident that Scheme 1 outperforms Scheme 2 at all six evaluation metrics, especially for the C_{DRR} indicator. The SOP significantly reduces the system load shedding ratio during peak load periods. Scheme 3 is slightly better than Scheme 1 in C_{ARP} , C_{VEI} , C_{ALR} , and C_{DDR} metrics since the probability of failure scenarios is low. In contrast to Schemes 1 and 2, Scheme 3 lacks planning consideration under fault scenarios, resulting in significantly larger values for the resilience indicators C_{FLR} and C_{AFR} . All in all, the proposed resilience-oriented planning of urban distribution system source–network–load–storage can improve the system economy under normal scenarios and resilience under fault scenarios.

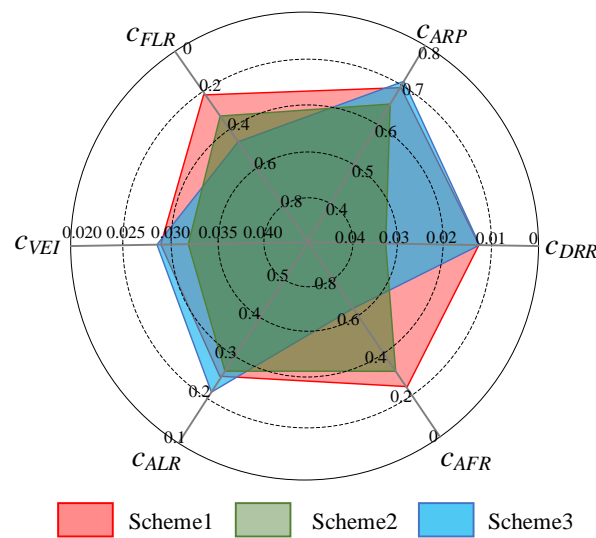


Figure 7. Multi-dimensional comparisons for Schemes 1–3.

5. Conclusions and Discussion

This paper proposes a resilience-oriented planning of urban distribution system source–network–load–storage in the context of high-penetrated building-integrated resources. It involves the location and capacity planning of RESs, network topology, EV charging stations, ESSs, SOPs, SVGs, and RCSs. Numerical studies have demonstrated that:

1. The contribution of SOP integration to system flexibility and thus to the system dependency on ESSs and SVGs results in a decrease in installed capacity. By exploiting the optimal synergies among different components, the coordination of source–network–load–storage can enhance the system dispatchability in spatial (RES accommodation) and temporal (energy storage) scales, thereby giving rise to at most 6.7% cost reduction.
2. SOPs have the capability to provide reactive voltage support and power flow transfer to the terminal nodes. By considering various fault scenarios during the planning stages, the node failure rates can be significantly reduced with the strengthened interconnectivity from SOPs, thereby mitigating the load losses incurred.
3. The proposed resilience-oriented planning scheme can outperform others on system economy, flexibility, and resilience indices, which exhibits huge development and application potentialities in urban distribution systems.

The limitations of this paper are the future multi-energy operation of urban distribution systems and the disturbances from various natural disasters, which are also our future works and directions:

1. Multi-energy source–network–load–storage coordination: Compared with power systems, gas and heating (cold) systems have larger time constants and significant time delays. The multi-energy source–network–load–storage coordination may need to be described by algebraic equations (electricity) and transient differential equations (gas, heat). With large-scale RES integration, multi-energy source–network–load–storage planning problems have evolved into problems involving multiple time scales of years, months/weeks, and short-term operations.
2. Disturbances from various natural disasters: Frequent natural disasters pose significant challenges to the urban distribution system, posing a severe threat to urban energy security and societal development. Worst of all is the combined impact of multiple weather- and climate-driven natural disasters, including typhoons, thunderstorms, floods, etc. Such disturbances from various natural disasters would contribute to considerable difficulty in pre-deployment and post-disaster recovery.

Author Contributions: Conceptualization, P.W.; Methodology, P.W.; Validation, S.Y.; Investigation, S.S.; Resources, W.L.; Data curation, T.L.; Writing—original draft, S.Z.; Writing—review and editing, S.X.; Supervision, X.Y.; Project administration, S.Z.; Funding acquisition, S.Z. All authors have read and agreed to the published version of the manuscript.

Funding: This research was funded by the Bengbu Power Supply Company of State Grid Anhui Electric Power Co., Ltd. Science and Technology Innovation Project (No. B312L023000K).

Data Availability Statement: The data presented in this study are available on request from the corresponding author. The data are not publicly available due to privacy concerns.

Conflicts of Interest: Authors Sheng Zhu, Ping Wang, Shilin Shen, Tongtong Liu and Shu Yang were employed by the company Bengbu Power Supply Company of State Grid Anhui Electric Power Co., Ltd. Author Wei Lou was employed by the company Electric Power Research Institute of State Grid Anhui Electric Power Co., Ltd. The remaining authors declare that the research was conducted in the absence of any commercial or financial relationships that could be construed as a potential conflict of interest.

Nomenclature

Abbreviations

BIPVs	Building-integrated photovoltaics
BIWT	Building-integrated wind turbine
ESS	Energy storage system
EV	Electric vehicle
MILP	Mixed-integer linear programming
PV	Photovoltaic
RESs	Renewable energy sources
RCSs	Remote-controlled switches
SVG	Static var generator
SOP	Soft open point
WT	Wind turbine

Indices and sets

t, s	Index for time, scenario
i, j	Index for node and branch
Ω_s, Ω_f	Set of normal and fault scenarios
$\Omega_{wt}, \Omega_{pv}, \Omega_{svg}, \Omega_{es}$	Set of BIWT, BIPV, SVG, ESS candidate nodes
$\Omega_{sub}, \Omega_{esub}$	Set of constructable and expandable substation nodes
Ω_L, Ω_n	Set of lines and load candidate nodes
$\Omega_{ev}, \Omega_{ev,i}$	Set of EV charging station nodes and candidate nodes

Parameters

K_i^{sop}, K_j^{sop}	Loss coefficients of SOP
$P_{i,t,s}^{WT}, P_{i,t,s}^{PV}$	BIWT and BIPV outputs
β_{min}, β_{max}	Lower and upper limits of SVG
$WT_i^{max}, PV_i^{max}, SVG_i^{max}, ES_i^{max}, S_i^{sop,max}$	Maximum installed capacities of BIWT, BIPV, SVG, ESS and SOP
$\lambda^{WT}, \lambda^{PV}$	Maximum allowable BIWT and BIPV curtailments
K^{sub}	Maximum load ratio of the substation
$S_i^{sub}, S_{i0}^{sub}, S_{ei}^{sub}$	Constructable, initial, and expandable substation capacities
n, n_{s0}, N	Total numbers of nodes, existing substations, and added nodes
ξ_i	Maximum load shedding ratio
$P_{i,t,s}^{LOAD}, Q_{i,t,s}^{LOAD}$	Active and reactive load
$k_{ch}, k_{dis}, \eta_{ch}, \eta_{dis}$	ESS charging and discharging depths and efficiency
μ_{min}, μ_{max}	Upper and lower bounds of ESS capacity
$P_{e,t,s}^{EV}$	EV charging station load
U_{min}, U_{max}, V_0	Minimum, maximum, and standard voltage
r_{ij}, x_{ij}, S_{ij}	Resistance, reactance and capacity of lines ij
$f_{ij,s}$	Fault of the line ij
R, R_{rcs}	Maximum numbers of restored lines and installed RCSs

T_f, T_{re}	Time of fault occurrence and recovery
$c_{wt}^{in}, c_{pv}^{in}, c_{es}^{in}, c_{sop}^{in}, c_{svg}^{in}, c_{rsc}^{in}, c_l^{in}, c_i^{esub}, c_i^{sub}$	Unit investment costs of BIWT, BIPVs, ESS, SOP, SVG, RCS, line constructed substation, and expanded substation
f_{wt}^{wt}, f_{pv}^{pv}	Penalties for BIWT and BIPV curtailment
f_{es}^{op}	Battery degradation cost
$c_{wt}^{op}, c_{pv}^{op}, c_{sop}^{op}, c_{svg}^{op}, c_l^{op}$	Annual maintenance costs of BIWT, BIPVs, SOP, SVG and line
f_i^t, F_i^{cut}	Load shedding penalties in normal and fault scenarios
ρ_s, ρ_{sf}	Probabilities in normal and fault scenarios
p_t	Exchange cost at the substation
Variables	
$P_{i,t,s}^{SOP}, Q_{i,t,s}^{SOP}, P_{i,t,s}^{SOP,loss}$	Active power, reactive power, and loss of SOP
S_i^{SOP}	SOP capacity
$n_{i,t,s}$	Binary variable for fault
$Q_{i,t,s}^{SVG}$	SVG reactive power output
WT_i, PV_i, SVG_i	Installed BIWT, BIPV, SVG capacities
$x_i^{WT}, x_i^{PV}, x_i^{ES}, x_i^{SVG}, x_i^{SOP}, x_{ij}^{RCS}$	Binary variables for BIWT, BIPV, ESS, SVG, SOP, and RCS installation
$P_{i,t,s}^{wt,use}, P_{i,t,s}^{pv,use}, P_{i,t,s}^{WT}, P_{i,t,s}^{pv,use}, P_{i,t,s}^{pv,gu}, P_{i,t,s}^{PV}$	Consumed, curtailed, and output power of BIWT and BIPV
x_i^{sub}, x_{ei}^{sub}	Binary variables for constructed and expanded substations
$P_{i,t,s}^{sub}, Q_{i,t,s}^{sub}$	Active and reactive power of substation
x_{ij}	Binary variable for constructed line
y_{ij}	Virtual flow from node i to node j
a_{ij}	Binary variable for installed RCS
$p_{i,t,s}^{cut}$	Curtailed power in normal scenarios
$P_{i,t,s}^{Fcut}, Q_{i,t,s}^{Fcut}$	Curtailed active and reactive power in fault scenario
$P_{i,t,s}^{ev}$	EV charging station load
$P_{i,t,s}^{dis}, P_{i,t,s}^{ch}, \eta_{i,t,s}^{ch}, \eta_{i,t,s}^{dis}$	ESS discharging and charging power and indicators
$S_{i,t,s}^{soc}$	ESS capacity
$x_{i,e}^{ev}$	Binary variable for installed EV charging station
$P_{i,t,s}^{ev}$	Power of the connected EV charging station
$P_{i,t,s}^{in}, Q_{i,t,s}^{in}, P_{ij,t,s}^{in}, Q_{ij,t,s}^{in}$	Active and reactive power injection
$U_{i,t,s}$	Voltage at node i
$x_{ij,t,s}^f$	Connection status for the fault

References

- Xu, D.; Wu, Q.; Zhou, B.; Li, C.; Bai, L.; Huang, S. Distributed multi-energy operation of coupled electricity, heating, and natural gas networks. *IEEE Trans. Sustain. Energy* **2019**, *11*, 2457–2469. [[CrossRef](#)]
- Xu, D.; Zhou, B.; Wu, Q.; Chung, C.Y.; Li, C.; Huang, S.; Chen, S. Integrated modelling and enhanced utilization of power-to-ammonia for high renewable penetrated multi-energy systems. *IEEE Trans. Power Syst.* **2020**, *35*, 4769–4780. [[CrossRef](#)]
- Wang, L.; Zhou, Y.; Xu, D.; Lai, Q. Fixed-/preassigned-time stability control of chaotic power systems. *Int. J. Bifurcat. Chaos* **2023**, *33*, 2350110. [[CrossRef](#)]
- Gao, H.; Wang, X.; Wu, K.; Zheng, Y.; Wang, Q.; Shi, W.; He, M. A review of building carbon emission accounting and prediction models. *Buildings* **2023**, *13*, 1617. [[CrossRef](#)]
- Zhang, Y.; Vand, B.; Baldi, S. A review of mathematical models of building physics and energy technologies for environmentally friendly integrated energy management systems. *Buildings* **2022**, *12*, 238. [[CrossRef](#)]
- Mai, W.; Chung, C. Economic MPC of aggregating commercial buildings for providing flexible power reserve. *IEEE Trans. Power Syst.* **2015**, *30*, 2685–2694. [[CrossRef](#)]
- Jin, X.; Jia, H.; Mu, Y.; Li, Z.; Wei, W.; Yu, X.; Xu, X.; Wang, H. A Stackelberg game based optimization method for heterogeneous building aggregations in local energy markets. *IEEE Trans. Energy Mark. Policy Regul.* **2023**, *2023*, 3251325. [[CrossRef](#)]
- Xiang, S.; Xu, D.; Gao, M. Optimal portfolio of wind-solar-hydro hybrid renewable generation based on variable speed pumped storage. In Proceedings of the 2023 IEEE 6th International Electrical and Energy Conference, Hefei, China, 12–14 May 2023; pp. 2371–2376.

9. Xu, L.; Ruan, X.; Mao, C.; Zhang, B.; Luo, Y. An improved optimal sizing method for wind-solar-battery hybrid power system. *IEEE Trans. Sustain. Energy* **2013**, *4*, 774–785.
10. Park, H. A Stochastic Planning model for battery energy storage systems coupled with utility-scale solar photovoltaics. *Energies* **2021**, *14*, 1244. [[CrossRef](#)]
11. Calise, F.; Cappiello, F.L.; d’Accadia, M.D.; Vicidomini, M. Dynamic simulation, energy and economic comparison between BIPV and BIPVT collectors coupled with micro-wind turbines. *Energy* **2020**, *191*, 116439. [[CrossRef](#)]
12. Fontenot, H.; Dong, B. Modeling and control of building-integrated microgrids for optimal energy management—A review. *Appl. Energy* **2019**, *254*, 113689. [[CrossRef](#)]
13. Zhou, B.; Xu, D.; Li, C.; Chung, C.Y.; Cao, Y.; Chan, K.W.; Wu, Q. Optimal scheduling of biogas–solar–wind renewable portfolio for multicarrier energy supplies. *IEEE Trans. Power Syst.* **2018**, *33*, 6229–6239. [[CrossRef](#)]
14. Xu, D.; Bai, Z.; Jin, X.; Yang, X.; Chen, S.; Zhou, M. A mean-variance portfolio optimization approach for high-renewable energy hub. *Appl. Energy* **2022**, *325*, 119888. [[CrossRef](#)]
15. Xu, D.; Xiang, S.; Bai, Z.; Wei, J.; Gao, M. Optimal multi-energy portfolio towards zero carbon data center buildings in the presence of proactive demand response programs. *Appl. Energy* **2023**, *350*, 121806. [[CrossRef](#)]
16. Xu, D.; Zhong, F.; Bai, Z.; Wu, Z.; Yang, X.; Gao, M. Real-time multi-energy demand response for high-renewable buildings. *Energy Build.* **2023**, *281*, 112764. [[CrossRef](#)]
17. Mansouri, S.A.; Ahmarinejad, A.; Sheidaei, F.; Javadi, M.S.; Jordehi, R.; Nezhad, A.E.; Catalo, J.P.S. A multi-stage joint planning and operation model for energy hubs considering integrated demand response programs. *Int. J. Electr. Power Energy Syst.* **2022**, *140*, 108103. [[CrossRef](#)]
18. Ahmarinejad, A. A multi-objective optimization framework for dynamic planning of energy hub considering integrated demand response program. *Sustain. Cities Soc.* **2021**, *74*, 103136. [[CrossRef](#)]
19. Zhang, C.; Li, J.; Zhang, Y.J.; Xu, Z. Optimal location planning of renewable distributed generation units in distribution networks: An analytical approach. *IEEE Trans. Power Syst.* **2017**, *33*, 2742–2753. [[CrossRef](#)]
20. Asensio, M.; Muñoz-Delgado, G.; Contreras, J. Bi-level approach to distribution network and renewable energy expansion planning considering demand response. *IEEE Trans. Power Syst.* **2017**, *32*, 4298–4309. [[CrossRef](#)]
21. Zheng, Y.; Song, Y.; Huang, A.; Hill, D.J. Hierarchical optimal allocation of battery energy storage systems for multiple services in distribution systems. *IEEE Trans. Sustain. Energy* **2019**, *11*, 1911–1921. [[CrossRef](#)]
22. Cao, Y.; Zhou, B.; Chung, C.Y.; Shuai, Z.; Hua, Z.; Sun, Y. Dynamic modelling and mutual coordination of electricity and watershed networks for spatio-temporal operational flexibility enhancement under rainy climates. *IEEE Trans. Smart Grid.* **2023**, *14*, 3450–3464. [[CrossRef](#)]
23. Xu, D.; Bai, Z.; Wang, T.; Zhuang, W. A centralized battery energy storage based medium-voltage multi-winding DVC for balance and unbalance operations. *IEEE Trans. Ind. Electron.* **2023**, *70*, 11898–11910. [[CrossRef](#)]
24. Yang, X.; Song, Z.; Wen, J.; Ding, L.; Zhang, M.; Wu, Q.; Cheng, S. Network-constrained transactive control for multi-microgrids-based distribution networks with soft open points. *IEEE Trans. Sustain. Energy* **2023**, *14*, 1769–1783. [[CrossRef](#)]
25. Li, P.; Ji, J.; Ji, H.; Song, G.; Wang, C.; Wu, J. Self-healing oriented supply restoration method based on the coordination of multiple SOPs in active distribution networks. *Energy* **2020**, *195*, 116968. [[CrossRef](#)]
26. Pamshetti, V.B.; Singh, S.P. Coordinated allocation of BESS and SOP in high PV penetrated distribution network incorporating DR and CVR schemes. *IEEE Syst. J.* **2022**, *16*, 420–430. [[CrossRef](#)]
27. Yang, X.; Xu, C.; Wen, J.; Zhang, Y.; Wu, Q.; Zuo, W.; Cheng, S. Cooperative repair scheduling and service restoration for distribution systems with soft open points. *IEEE Trans. Smart Grid.* **2023**, *14*, 1827–1842. [[CrossRef](#)]
28. Zhang, J.; Foley, A.; Wang, S. Optimal planning of a soft open point in a distribution network subject to typhoons. *Int. J. Electr. Power Energy Syst.* **2021**, *129*, 106839. [[CrossRef](#)]
29. Tari, A.N.; Sepasian, M.S.; Kenari, M.T. Resilience assessment and improvement of distribution networks against extreme weather events. *Int. J. Electr. Power Energy Syst.* **2021**, *125*, 106414. [[CrossRef](#)]
30. Salimi, M.; Nasr, M.A.; Hosseini, S.H.; Gharehpetian, G.B.; Shahidepour, M. Information gap decision theory-based active distribution system planning for resilience enhancement. *IEEE Trans. Smart Grid.* **2020**, *11*, 4390–4402. [[CrossRef](#)]
31. Poudyal, A.; Poudel, S.; Dubey, A. Risk-based active distribution system planning for resilience against extreme weather events. *IEEE Trans. Sustain. Energy* **2022**, *14*, 1178–1192. [[CrossRef](#)]
32. Qin, Q.; Han, B.; Li, G.; Wang, K.; Xu, J.; Luo, L. Capacity allocations of SOPs considering distribution network resilience through elastic models. *Int. J. Electr. Power Energy Syst.* **2022**, *134*, 107371. [[CrossRef](#)]
33. Yang, X.; Zhou, Z.; Zhang, Y.; Liu, J.; Wen, J.; Wu, Q.; Cheng, S.-J. Resilience-oriented co-deployment of remote-controlled switches and soft open points in distribution networks. *IEEE Trans. Power Syst.* **2022**, *38*, 1350–1365. [[CrossRef](#)]
34. Ma, L.; Wang, L.; Liu, Z. Soft open points-assisted resilience enhancement of power distribution networks against cyber risks. *IEEE Trans. Power Syst.* **2022**, *38*, 31–41. [[CrossRef](#)]

35. Lofberg, J. YALMIP: A toolbox for modeling and optimization in MATLAB. In Proceedings of the 2004 IEEE International Conference on Robotics and Automation (IEEE Cat. No. 04CH37508), Taipei, Taiwan, 2–4 September 2004; pp. 284–289.
36. Li, Z.; Wu, W.; Tai, X.; Zhang, B. A reliability-constrained expansion planning model for mesh distribution networks. *IEEE Trans. Power Syst.* **2020**, *36*, 948–960. [[CrossRef](#)]

Disclaimer/Publisher’s Note: The statements, opinions and data contained in all publications are solely those of the individual author(s) and contributor(s) and not of MDPI and/or the editor(s). MDPI and/or the editor(s) disclaim responsibility for any injury to people or property resulting from any ideas, methods, instructions or products referred to in the content.